Nanoscale

COMMUNICATION

View Article Online
View Journal | View Issue



Cite this: *Nanoscale*, 2018, **10**, 20131

Received 29th August 2018,
Accepted 18th October 2018

DOI: 10.1039/c8nr07022a

rsc.li/nanoscale

# Silica coating enhances the stability of inorganic perovskite nanocrystals for efficient and stable down-conversion in white light-emitting devices†

Fei Zhang,[a] Zhi-Feng Shi, *[a] Zhuang-Zhuang Ma,[a] Ying Li,[a] Sen Li,[a] Di Wu,[a] Ting-Ting Xu,[a] Xin-Jian Li,*[a] Chong-Xin Shan[a,b] and Guo-Tong Du[c]

**Recently, inorganic halide perovskite ($CsPbX_3$, X = Cl, Br, I) quantum dots (QDs) have attracted tremendous research interests because of their great potential for application in the fields of low-cost light sources and displays. However, the unsatisfactory structural and chemical stabilities of such materials are the main obstacles hindering reliable device operation significantly. In this study, we successfully prepared $CsPbBr_3$/silica QD composites through a simple sol–gel reaction by using tetramethoxysilane as a single molecule precursor. The as-prepared $CsPbBr_3$/silica QD composites demonstrated substantially improved stability against heat, light, and environmental oxygen/moisture. Besides, a relatively narrower photoluminescence linewidth and higher quantum yield were achieved compared with that of fresh $CsPbBr_3$ QDs. Furthermore, the $CsPbBr_3$ QDs/silica composites were applied as color-converting layer curing on blue light-emitting diodes (LEDs) for white LED applications. Finally, a high power efficiency of 63.5 lm $W^{-1}$ was obtained and the light emission could be efficiently sustained over 13 h without any decay in the continuous current mode, demonstrating remarkable operation stability than that reported previously. It can be anticipated that the excellent properties and facile processing technique used here will make perovskite QDs/silica composites attractive for applications in optoelectronics and industrial fields.**

## Introduction

Nowadays, nearly 25% of the global electricity consumption is used for lighting, which is responsible for more than 6% carbon dioxide emissions each year.[1,2] To change the way we light our houses and businesses under this circumstance, white light-emitting devices (WLEDs) are becoming prevalent because of their higher power efficiency than the frequently used fluorescent lamps and incandescent bulbs.[3] Besides, other advantages offered by WLEDs include high luminous efficiency, fast response, long lifetime, and compact size.[4–6] At present, the commercialization route for WLED production involves the combination of a blue-emissive LED chip with the $Y_3Al_{15}O_{12}:Ge^{3+}$ phosphor because it has the advantages of low cost, simple structure, and high luminous efficiency.[7] However, this strategy lacks the red and green light components and is not sufficient to produce a wide color gamut as it relies solely on the blue light and the wide yellow spectrum.[5,8]

Recently, inorganic halide perovskite ($CsPbX_3$, X = Cl, Br, I) quantum dots (QDs) have attracted tremendous research interests because of their exceptional optoelectronic properties, demonstrating great application potentials in the fields of low-cost light sources and displays.[9–17] In 2016, Snaith and colleagues pioneered an approach for white light sources by using perovskite QDs as the down-conversion phosphors.[18] Since then, the progress of this strategy has been developing in the past two years. However, the well-known instability issue of halide perovskites is the major obstacle for their commercialization and mass production. Especially, perovskite QDs have to be processed into a layer or composite, and they also have to be exposed to an external illuminant source for a long period. Therefore, the development of a manufacturing process that is simple, easy, and repeatable to improve the material stability while retaining high optical quality is highly desired and certainly worth exploring.[19] A straightforward approach to enhance the stability of perovskite QDs is to coat the QD core with an inert and robust shell, and it has made significant progress very recently. Palazon and colleagues demonstrated an approach to improve the stability by cross-linking the C=C double bond structure of the surface ligands by X-ray irradiation of perovskites.[20] Kanaras *et al.* proposed to increase the chemical and optical stability of perovskite QDs by the syn-

[a]*Key Laboratory of Materials Physics of Ministry of Education, Department of Physics and Engineering, Zhengzhou University, Zhengzhou 450052, China. E-mail: shizf@zzu.edu.cn, lixj@zzu.edu.cn; Fax: +86-371-67766629; Tel: +86-150-9333-9165*

[b]*State Key Laboratory on Luminescence and Applications, Changchun Institute of Optics, Fine Mechanics and Physics, Chinese Academy of Sciences, Changchun 130033, China*

[c]*State Key Laboratory on Integrated Optoelectronics, College of Electronic Science and Engineering, Jilin University, Qianjin Street 2699, Changchun 130012, China*

†Electronic supplementary information (ESI) available. See DOI: 10.1039/c8nr07022a

thesis of poly(maleic anhydride-alternate-1-octadecene) to QDs.[21] Also, there are some methods for encapsulating perovskite QDs in organic polymers, such as polymethyl methacrylate, to achieve good processability and compatibility with typical packaging methods.[12,15,22,23] However, under certain conditions, such as ultraviolet (UV) light, organic polymers have relatively poor stability and lose their ability against photo-oxidation after a short time.[24] In contrast, an inorganic matrix has better mechanical properties and tightness. Because of the low diffusion rate of atoms or ions, inorganic silicon oxide, aluminum oxide, and titanium oxide have been frequently employed as barriers to protect organic LEDs and phosphors from moisture/oxygen degradation.[25–28] More recently, some examples of perovskite QD encapsulation have been demonstrated successfully. For instance, the mesoporous $CsPbX_3$/silica QD nanocomposites prepared by Liu's team showed good light stability and thermal stability.[29] Zeng *et al.* prepared $CsPbBr_3$@$Cs_4PbBr_6$/$SiO_2$ QD nanocomposites with an improved stability and further demonstrated their applications in anti-counterfeiting.[30] Loiudice *et al.* reported the enhancement of material stability against environment oxygen/moisture, light and heat by encapsulating $CsPbBr_3$ QDs within an alumina matrix by atom layer deposition.[31] However, in their cases, most of the products were characterized by large aggregates with multiple perovskite QDs encapsulated into one oxide shell, inevitably hindering some important applications required for the use of monodisperse particles.[32]

Following this line of thought, we developed a facile approach to substantially improve the stability of $CsPbBr_3$ QDs by *in situ* addition of tetramethoxysilane (TMOS) as a single molecule precursor at room temperature (RT). The obtained $CsPbBr_3$/silica QD composites are characterized as uniformly distributed monodisperse particles without the formation of large aggregates. Compared with the results of fresh $CsPbBr_3$ QDs, a substantially enhanced material stability against heat, light, and environmental oxygen/moisture was achieved. Besides, a narrower photoluminescence (PL) linewidth and a higher PL quantum yield for silica-coated $CsPbBr_3$ QDs were demonstrated. Furthermore, the obtained $CsPbBr_3$/silica QD composites were employed as solid state phosphors in WLED fabrication, and the device performance was remarkable with a high power efficiency of 63.5 lm $W^{-1}$. More importantly, the proposed WLEDs demonstrated remarkable operation stability in the continuous current mode. Even when operated in air ambience, the light emission could be efficiently sustained over 13 h without any decay, which was much superior to the results of the reference device with bare $CsPbBr_3$ QD powder as green phosphors. The results obtained prove that our strategy is an effective strategy for enhancing the material stability for perovskite QDs, thus opening up enormous opportunities for their applications in lighting and display fields.

## Experimental

Here, a simple processing approach was employed to prepare silica-coated $CsPbBr_3$ QD composites at RT and normal pressure conditions, and the corresponding processing procedures are illustrated in Fig. 1. First, $PbBr_2$ (0.2 mmol), CsBr (0.4 mmol), oleic acid (OA, 0.5 mL), and oleylamine (OAm, 0.25 mL) were added to *N*,*N*-dimethylformamide (DMF, 5 mL) under 400 rpm stirring to form a precursor solution. Please note that OA and OAm serve as the surfactants in the synthesis process to control the dimension and surface states of the products, allowing the formation of zero-dimensional $CsPbBr_3$ QDs with a high PL quantum yield. Second, 0.5 mL of the precursor solution was rapidly injected into toluene solution (5 mL) under 700 rpm stirring, forming $CsPbBr_3$ nanocrystals immediately. Third, the $CsPbBr_3$ QD solution was centrifuged at 7000 rpm for 10 min, and the resulting precipitate was redissolved in toluene solution. Following this, a certain amount of TMOS solution was added into the $CsPbBr_3$ QD solution and allowed to stand in a natural environment for 72 h. It is generally recognized that the cross-linking can enhance the stability of QD-silica monolith, especially after thermal annealing treatment, which is associated with a more densely cross-linked structure that acts as a barrier to effectively prevent oxygen and moisture from reaching QDs.[33] Therefore, in our case, $CsPbBr_3$/$SiO_2$ QDs were pre-annealed for half an hour at 40 °C. Through this process, $CsPbBr_3$ QDs were successfully incorporated into the $SiO_2$ monolith by a simple sol–gel method. In this case, the "waterless" toluene solution played a crucial role mainly considering the following three aspects: (1) The toluene solution can be considered to have anti-solvent compatibility as it aids the formation of zero-dimensional $CsPbBr_3$ QDs. (2) A low-water content (analytical grade, $H_2O$ content 0.0184%) in the toluene solution favors the hydrolysis reaction of TMOS, thereby enabling the formation of an $SiO_2$ layer on perovskite QDs. Thus, the $SiO_2$ monolithic material was prepared without adding any catalyst in the solution, as represented by the following reaction:

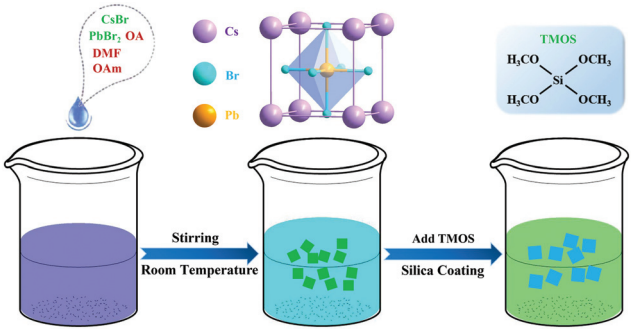


Fig. 1 Schematic diagram illustrating the coating process for the preparation of $CsPbBr_3$/$SiO_2$ QDs.

$$Si(OCH_3)_4 + 2H_2O \rightarrow SiO_2 + 4CH_3OH \quad (1)$$

(3) The compatibility of non-polar toluene with $CsPbBr_3$ and TMOS facilitates the encapsulation of QDs in $SiO_2$ without the need for aggregation. In previous studies, tetramethyl orthosilicate (TEOS) was frequently employed as the precursor to achieve $SiO_2$ coating on the perovskite QDs by a hydrolysis

 

reaction.[34] However, most efforts failed because the perovskite QDs were easily decomposed by water before $SiO_2$ generation, which is due to the higher hydrolysis rate of TMOS than that of TEOS. Therefore, TMOS is a better choice for coating silica onto perovskite QDs without degrading their original optical and structural properties. Experimentally, TEOS-treated $CsPbBr_3$ QDs were prepared, and clearly decreased PL intensity after treatment and poor moisture stability of $CsPbBr_3$/silica QD composites indicated that TEOS is not suitable for silica coating (Fig. S1, ESI†).

The microstructures of $CsPbBr_3$ QDs before and after TMOS coating were examined by transmission electron microscopy (TEM). Fig. 2a shows typical TEM images of the as-synthesized $CsPbBr_3$ QDs, which are characterized as uniformly distributed cubic particles. The diameter of $CsPbBr_3$ QDs is in the range of 7.5–13.6 nm with an average size of 11.7 nm, as shown in Fig. 2e. From the high-resolution TEM image presented in Fig. 2b, a well-defined crystalline structure with a characteristic lattice plane distance of ~0.58 nm can be observed, corresponding to the *d*-spacing of (200) crystal plane of cubic $CsPbBr_3$. The corresponding Fourier transformation (FFT) image shown in Fig. 2c confirms the single-crystalline nature of $CsPbBr_3$ QDs. After the TMOS coating process, the cubic shape of $CsPbBr_3$ QDs remains unchanged and the dispersion of QDs is almost unaffected (Fig. 2d). However, the average size of these cubes increases from 11.7 to 12.8 nm (Fig. 2f), implying that the silica coating has taken effect. Other possible factors causing an increase in size cannot be unambiguously ruled out at present; for instance, excess TMOS that is not removed completely by the purification process is also prone to attach to the surface of QDs, and/or the continuous growth of the nanocrystals with unreacted precursors before the $SiO_2$ matrix is complete in this sol–gel reaction process.[35] In any case, the substantially improved stability of the $CsPbBr_3$/silica QD composites against environmental oxygen/moisture, light and heat as discussed later manifests that this method provides a successful surface protection strategy for perovskite QDs. Please note that the microstructure characteristics of $CsPbBr_3$/silica QD composites cannot be distinguished well from the TEM results unlike other previous results.[35,36] This is because $CsPbBr_3$ QDs in our case are characterized by a cubic shape and have a lower surface energy than $CsPbBr_3$ QDs with a spherical shape. In the present case, during TMOS coating, $SiO_2$ oligomer remains in solution instead of growing on the surface of large nanocubes, forming free silica. For spherical $CsPbBr_3$ QDs, $SiO_2$ oligomers tend to grow on the surface of QDs because of their relatively higher surface energy and the absence of the self-assembly effect. In addition, the chemical composition of $CsPbBr_3$ QDs before and after TMOS coating is determined by energy dispersive X-ray spectroscopy (EDS)

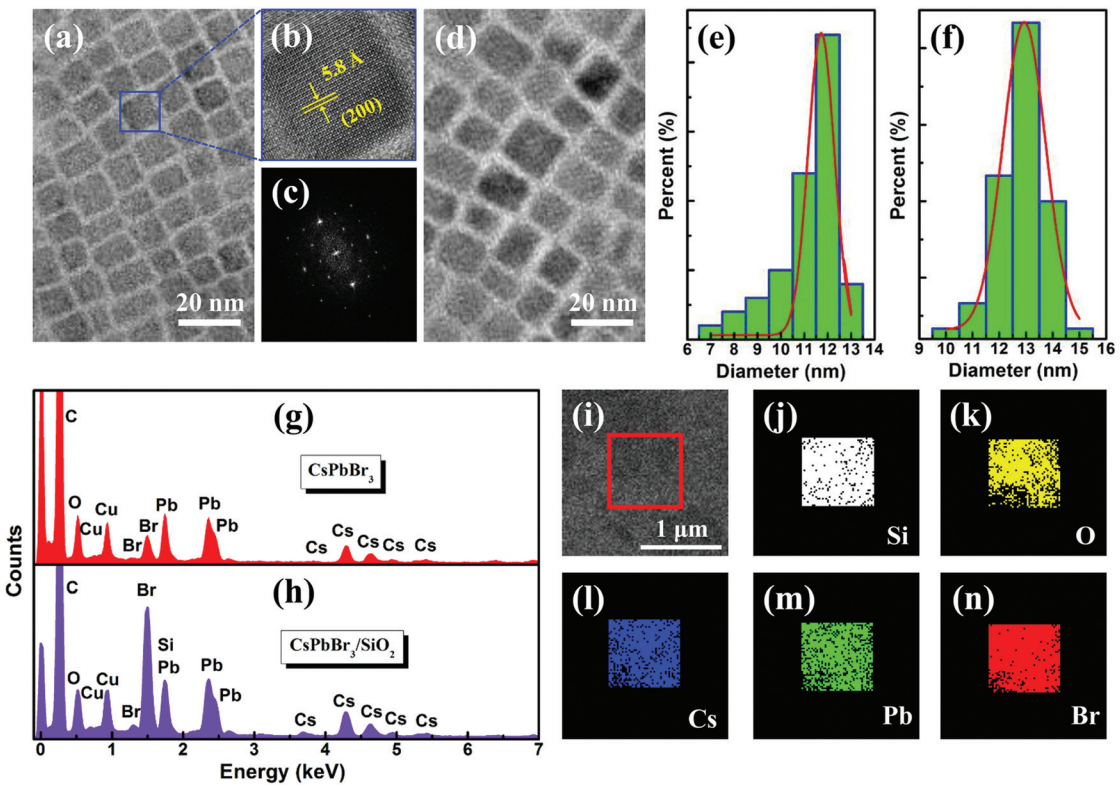


Fig. 2 (a) TEM images of fresh $CsPbBr_3$ QDs. (b) High-resolution TEM image of $CsPbBr_3$ QDs showing a characteristic lattice plane distance of 0.58 nm. (c) FFT image corresponding to (b). (d) TEM images of $CsPbBr_3/SiO_2$ composites. Histograms for the size distribution of the $CsPbBr_3$ QDs (e) before and (f) after TMOS coating. EDS spectra of (g) $CsPbBr_3$ QDs and (h) $CsPbBr_3/SiO_2$ QDs. (i–n) Elemental mapping analysis showing the elemental distribution of silicon, oxygen, cesium, lead, and bromine, respectively.

measurements. As shown in Fig. 2g and h, in addition to the well-known compositions of Cs, Pb, Br, Cu, and O, Si is also identified, confirming the formation of $CsPbBr_3$/silica QD composites. Further analysis of the EDS elemental mapping of the $CsPbBr_3$/silica QD films is performed by employing Si, O, Cs, Pb, and Br as detection signals. It is apparent that the five target elements are uniformly distributed throughout the selected square area marked in Fig. 2i, thus demonstrating that $CsPbBr_3$ QDs are successfully and uniformly encapsulated in the silica matrix.

Furthermore, we compared the optical properties of $CsPbBr_3$ QDs before and after TMOS coating by UV-visible absorption and PL measurements at RT. As shown in Fig. 3a, the absorption spectra of the two samples showed no significant changes, but a clear red-shift of 4.5 nm of the PL emission peak was observed after TMOS coating. The full-width at half-maximum (FWHM) value of the emission peak was slighted reduced by 13.6 meV after TMOS coating, and the symmetric spectra shape could be maintained without any noticeable sub-bandgap emission associated with the defects in perovskites. Besides, the emission intensity of $CsPbBr_3$/silica QD composites increased by 30% in comparison with that of the fresh counterpart, which may be due to the reduced charge-carrier trapping states after silica passivation, which are generally used as relaxation pathways. Excellent emission performance with improved color purity is a signature of high-quality $CsPbBr_3$/silica QD composites with low defect density, making the materials suitable as effective green emitters for luminescent device applications. Please note that the red-shift phenomenon in the PL emission for the TMOS-treated $CsPbBr_3$ QDs is difficult to understand because the quantum confinement effect exists even after silica coating. Also, FWHM narrowing and PL enhancement for $CsPbBr_3/SiO_2$ QD composites have confirmed this view. Herein, we consider that two factors can be responsible for the red-shift behavior of PL emission. On the one hand, during the TMOS coating process, continuous growth of $CsPbBr_3$ core with unreacted precursors can occur before the $SiO_2$ matrix is completely formed in the sol–gel reaction process. Even if the continuous growth of $CsPbBr_3$ core is not clear, a slight red-shift of the PL emission will be induced, as reported in Sun's study.[35] On the other hand, some other previous studies have recognized that the increased re-absorption effect of $CsPbBr_3/SiO_2$ QD composites can also induce a PL red-shift.[37,38] To gain more insights into the carrier recombination dynamics of the perovskite products, time-resolved PL measurements were performed. Fig. 3b presents the PL decay curves of $CsPbBr_3$ QDs before and after TMOS coating, which can be well-fitted to a bi-exponential decay function. The average lifetime ($\tau_{ave}$) of $CsPbBr_3$/silica QD composites was calculated to be 7.8 ns, which was longer than that of the fresh $CsPbBr_3$ QD counterpart (4.3 ns). The longer lifetime after TMOS coating indicates efficient suppression of nonradiative recombination paths by surface passivation. In other words, the trapping of excited electrons by the surface states is inhibited. Thus, the efficient usage of excited carriers is favored, resulting in a high PL quantum yield as well as a long lifetime.

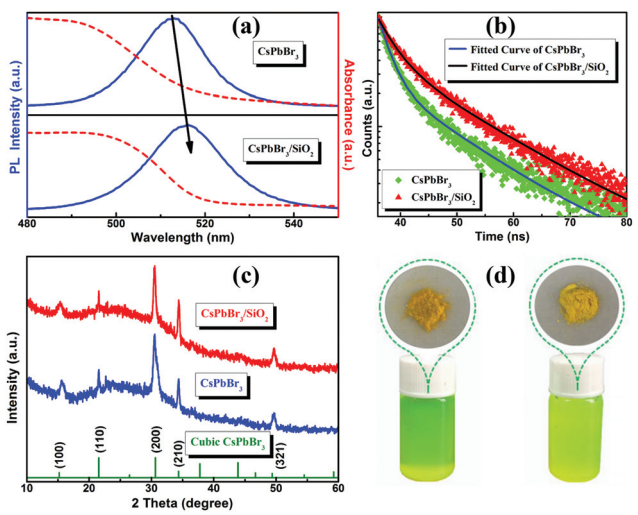


Fig. 3 (a) Comparison of the absorption and PL spectra of fresh $CsPbBr_3$ QDs and $CsPbBr_3/SiO_2$ QD composites. (b) Time-resolved PL decay and fitting curves of fresh $CsPbBr_3$ QDs and $CsPbBr_3/SiO_2$ QD composites. (c) XRD patterns of $CsPbBr_3$ QDs before and after TMOS coating, and the standard XRD patterns of the cubic phases of $CsPbBr_3$. (d) Solutions and powders of fresh $CsPbBr_3$ QDs (left) and $CsPbBr_3/SiO_2$ QD composites (right).

Fig. 3a displays the X-ray diffraction (XRD) patterns of as-synthesized and silica-coated $CsPbBr_3$ QDs. It can be seen that both samples showed a cubic perovskite structure; characteristic and dominant diffraction peaks corresponding to (100), (110), (200), (210) and (321) planes were observed. This indicated that both the samples preferentially assembled in the (200) and (210) planes during film formation, and $CsPbBr_3$ QDs did not change significantly during the sol–gel reaction with TMOS addition. Fig. 3d presents pure $CsPbBr_3$ QD solution (powder) before and after TMOS coating. After being wrapped by silica, the color of the solution gradually changed from green to kelly green, and the corresponding PL quantum yield increased slightly from 55% to 72%, which was consistent with the above discussions on steady/transient-state PL results. Moreover, the pure $CsPbBr_3$ QD powder was yellow and that with TMOS treatment was pale yellow. The relatively dark and light colors are probably due to the sensitivity of $CsPbBr_3$ QDs to the surrounding environment and the $SiO_2$ matrix.[37]

To better understand the optical recombination mechanisms of $CsPbBr_3$ QDs before and after the TMOS treatment, temperature-dependent PL measurements were further obtained in the temperature range of 10–300 K. As presented in Fig. 4a and b, with the increase in temperature, only one emission peak can be resolved for two samples, implying that no structural phase transition occurs within the heating process (10–300 K). Besides, the emission intensities of both samples exhibit a decreasing trend accompanied by a monotonous blue-shift of the emission peak. It should be mentioned that the blue-shift phenomenon is unusual and may be related

 

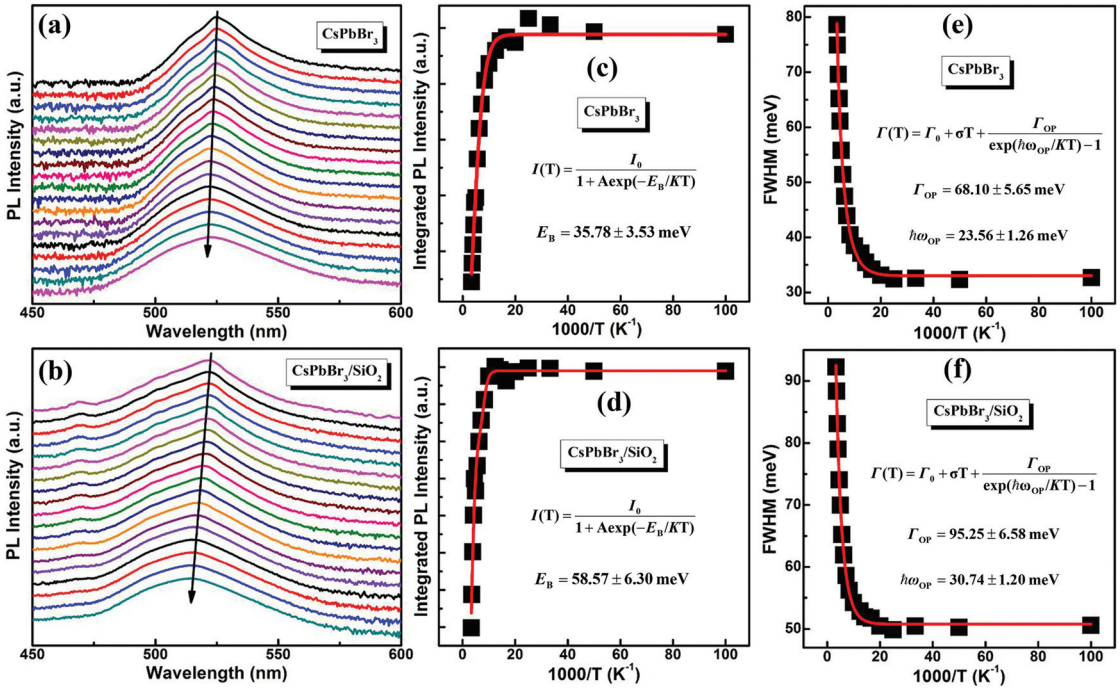


**Fig. 4** Temperature-dependent PL spectra of (a) the $CsPbBr_3$ QDs and (b) $CsPbBr_3/SiO_2$ QD composites taken from 10 to 300 K. The relationship between the integrated PL intensity and the reciprocal temperature from 10 to 300 K for (c) $CsPbBr_3$ QDs and (d) $CsPbBr_3/SiO_2$ QD composites. FWHM of (e) $CsPbBr_3$ QDs and (f) $CsPbBr_3/SiO_2$ QD composites as a function of reciprocal temperature.

to the thermal expansion of the crystal lattice through the process of increasing temperature and electron–phonon renormalization. The temperature quenching behavior of the PL emission intensity for two samples can be due to the thermally activated nonradiative recombination process, and the integrated PL intensity values can be well-fitted by the following formula:[39]

$$I(T) = \frac{I_0}{1 + A\exp\left(-\frac{E_B}{KT}\right)} \quad (2)$$

Here, $I_0$ is the emission intensity at 10 K, $E_B$ is the exciton binding energy, $A$ is the fitted constant, and $K$ is the Boltzmann constant. As displayed in Fig. 4c and d, the fitting curves produce $E_B$ values of 35.78 ± 3.53 meV and 58.57 ± 6.30 meV for fresh $CsPbBr_3$ QDs and $CsPbBr_3/SiO_2$ QD composites, respectively. Therefore, after encapsulation by silica, $E_B$ of perovskite QDs increases. In theory, relatively higher $E_B$ than the thermal ionization energy at RT (~26 meV) ensures the survival of excitons well above RT and a high rate of recombination. Thus, the excitonic emission can be efficiently sustained even when the $CsPbBr_3/SiO_2$ QD composites are excited at a higher temperature; this suggests improved temperature tolerance of $CsPbBr_3$ QDs after TMOS coating and indicates additional potentials of such materials in exciton-related optoelectronic devices. In addition, detailed analysis on the temperature-dependent PL peak broadening behavior can provide information on the exciton–phonon interaction in perovskite QDs. As shown in Fig. 4e and f, the FWHM values of PL emission peaks at different temperature points were fitted using the independent Boson model:[40]

$$\Gamma(T) = \Gamma_0 + \sigma T + \frac{\Gamma_{op}}{\exp(\hbar\omega_{op}/KT) - 1} \quad (3)$$

Here, $\Gamma_0$ is the non-uniform linewidth, which does not change with temperature and depends on the shape, size, and composition of inhomogeneous QDs; $\sigma$ is the exciton–acoustic phonon interaction, $\Gamma_{op}$ is the exciton-optical fitting coefficient (contribution to FWHM broadening), and $\hbar\omega_{op}$ is the optical phonon energy. From the equation, one can observe that $\Gamma_0$ is the main contributor to $\Gamma(T)$ at low temperatures, and the contribution from acoustic and optical phonons is larger than $\Gamma_0$ at relatively higher temperatures, which ultimately leads to a nonlinear increase in FWHM. Finally, the $\hbar\omega_{op}$ values of fresh $CsPbBr_3$ QDs and $CsPbBr_3/SiO_2$ QD composites were fitted to be 23.5 and 30.74 meV, respectively. Therefore, after silica coating, the optical phonon energy of $CsPbBr_3$ QDs increases. The relatively stronger exciton–phonon interaction of the $CsPbBr_3/SiO_2$ QD composites indicates improved and desired thermal antiquenching effects required at high temperatures.[41] Thus, the silica-coated perovskite QDs can be expected to operate with good stability.

As is well-known, the stability of halide perovskites has always been criticized as the main obstacle hindering their potential applications significantly. In this study, the environmental stability of $CsPbBr_3/SiO_2$ QD composites was assessed by investigating the effects of heat, water, and UV light irradiation on the optical properties of TMOS-coated products.

To compare the thermal stability of $CsPbBr_3$ QDs before and after TMOS coating, thermal cycling measurements were performed in the temperature range of 20–120 °C, and the integrated PL intensity was normalized for comparison. As shown in Fig. 5a and b, the relative PL intensity decreased gradually with increasing temperature owing to fluorescence quenching (heating process, cycle I) for both samples, but their decay extents were radically different. In contrast, the emission intensity of fresh $CsPbBr_3$ QDs decreased sharply with increasing temperature, and a rather large emission decay of ~51.1% was observed after the cooling process (cooling/cycle 1), whereas that of silica-coated $CsPbBr_3$ QDs was only ~12.94%. The unrecoverable behavior of the PL performance may be related to the additional structural defects in fresh $CsPbBr_3$ QDs and $CsPbBr_3/SiO_2$ QD composites caused by heating; thus, the radiative recombination probability of photo-generated carriers was reduced accordingly. An additional observation is that the magnitude of PL intensity decay slightly decreased after the cooling processes of cycles 2 and 3. After three successive heating/cooling measurement cycles, the PL intensity showed 15.5% decay altogether for $CsPbBr_3/SiO_2$ QD composites. Compared with the larger decay above 66% for the fresh $CsPbBr_3$ QDs, a substantially improved thermal stability was demonstrated for the silica-coated sample, thus opening up enormous opportunities for obtaining high-performance optoelectronic devices with good temperature tolerance. Even after six heating/cooling measurement cycles, ~82% of the initial emission intensity was maintained for $CsPbBr_3/SiO_2$ QD composites. As summarized in Fig. 5d with two representative temperature points (20 and 120 °C), clearly superior performance of silica-coated QDs was observed compared to that of fresh $CsPbBr_3$ QDs, in which only 25% of the original emission was retained (Fig. 5c). Because TMOS plays a positive role in deactivating the defect states on the surface of perovskite QDs, it seems reasonable that the luminescence quenching phenomenon of the $CsPbBr_3/SiO_2$ QD composites is effectively suppressed.

To further assess the moisture stability of $CsPbBr_3$ QDs after TMOS coating, 20 μL of deionized water was added into the QD solution (1 mL, toluene), and the corresponding PL intensity was monitored at time intervals of 10 min. For comparison, the measurement results of fresh $CsPbBr_3$ QDs were also obtained. As shown in Fig. 6a, fresh $CsPbBr_3$ QDs experienced rapid fluorescence quenching after the addition of deionized water into the toluene solution, retaining only 15% of the initial intensity after 3 h storage. In sharp contrast, when the $CsPbBr_3/SiO_2$ QD composites were exposed to the same volume of deionized water, nearly 95% of the original PL performance was retained over 3 h of continuous test, which was much superior to that of fresh $CsPbBr_3$ QDs. Fig. S2 (ESI†) shows the corresponding PL spectra of the two samples recorded before and after the 3 h moisture stability test; except for the difference in their intensities, the peak position and FWHM of PL spectra were almost unchanged. The above results suggest that the moisture stability of $CsPbBr_3$ QDs after TMOS coating has been significantly enhanced. This is because the desirable $SiO_2$ shell encapsulates $CsPbBr_3$ QDs to achieve very low water permeability, thus preventing water molecules from entering the $CsPbBr_3$ QD core surface. Conversely, bare $CsPbBr_3$ QDs were easily decomposed owing to the hypersensitivity of lead perovskite materials in water or even in air with low moisture content.

Moreover, the photostability of the $CsPbBr_3/SiO_2$ QD composites was investigated by continuously illuminating the sample with a portable UV lamp with 10 cm distance, and the time interval for obtaining spectra was 1 h. As shown in

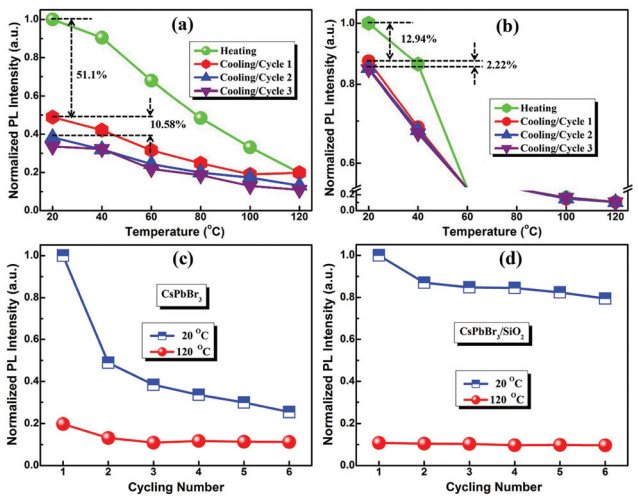


Fig. 5 Three thermal cycling measurements showing the thermal stability of (a) the fresh $CsPbBr_3$ QDs and (b) $CsPbBr_3/SiO_2$ QD composites. Plots of the normalized emission intensity of (c) fresh $CsPbBr_3$ QDs and (d) $CsPbBr_3/SiO_2$ QD composites at two representative temperature points (20 °C and 120 °C) over six thermal cycling measurements.

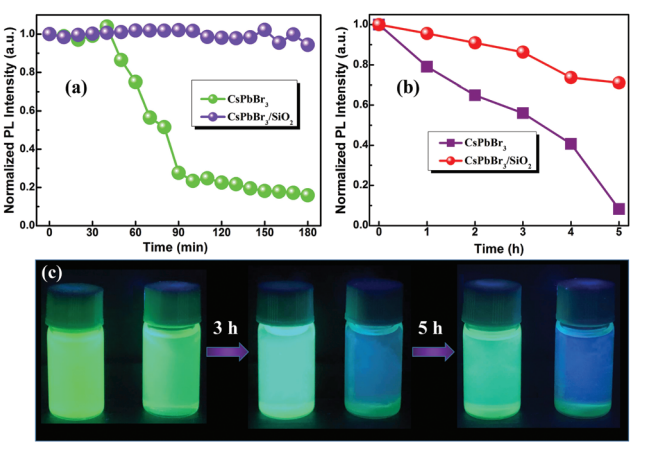


Fig. 6 (a) The relative PL intensities of fresh $CsPbBr_3$ QDs and $CsPbBr_3/SiO_2$ QD composites after adding 20 μL deionized water into the solution (1 mL, toluene). (b) Photostability test of fresh $CsPbBr_3$ QDs and $CsPbBr_3/SiO_2$ QD composites under continuous UV light irradiation (365 nm, 20 W). (c) Photographs of fresh $CsPbBr_3$ QDs (right) and $CsPbBr_3/SiO_2$ QD composites (left) at different time periods under UV light irradiation.

Fig. 6b, after irradiation for 5 h under a UV light, the $CsPbBr_3/SiO_2$ QD composites maintained ~72% of their initial performance. However, the relative emission intensity of fresh $CsPbBr_3$ QDs decreased to 8.2% of the original value (purple dotted line). Fig. 6c displays the corresponding photographs of fresh $CsPbBr_3$ QDs (right) and $CsPbBr_3/SiO_2$ QD composites (left) at different time periods under UV light irradiation. Although slight weakening of the emission intensity could be seen for the $CsPbBr_3/SiO_2$ QD composites, the sample was still strongly fluorescent. In comparison, fresh $CsPbBr_3$ QDs lost most of the brightness after 5 h UV light irradiation, gradually changing from green to transparent, corresponding to the above discussions on spectra (Fig. 6b). This is presumably because bare $CsPbBr_3$ QDs started to decompose gradually by photo-oxidation. As deduced from previous studies on core/shell structured II–VI semiconductor QDs,[42] the formation of a passivation shell can prevent undesirable photo-oxidation over continuous UV light irradiation. This suggests the great potential of silica-coated $CsPbBr_3$ QDs in reliable and environmentally friendly lighting applications. Please note that the TMOS coating method proposed in this study is also applicable to other $CsPbX_3$ QDs. We have employed this sol–gel reaction to coat $CsPbCl_3$ and $CsPbI_3$ QDs with TMOS, and substantially improved stability against heat, light, and environmental oxygen/moisture was also achieved, as presented in Fig. S3–S5 (ESI†).

To demonstrate the potential applications of $CsPbBr_3/SiO_2$ QD composites as down-conversion phosphors, a WLED was fabricated by encapsulating a mixture of the green-emissive $CsPbBr_3/SiO_2$ QD powder, red-emissive $K_2SiF_6:Mn^{4+}$ (KSF) phosphors and organic polymer silica gel above a blue-emissive LED chip, as shown in Fig. 7a. This packaging process is similar to the commercial packaging process. Please note that such a non-contact configuration for WLED fabrication in the present case has unique benefits compared with that of electrically driven LEDs that follow carrier injection mechanism; the phosphor layer is separated from the excitation LED p–n junction, and very less heat released from the bottom LED chip can be imposed on the upper phosphor because of the appreciable distance between the phosphor and LED chip. Moreover, the integrity of the p–n junction in the bottom LED could be effectively protected owing to the absence of undesirable disturbances caused by directly touching the phosphors. Therefore, generally, high-efficiency light emission can be sustained over a long time for such devices with a non-contact configuration. Fig. 7b and c show the emission of the down-conversion WLED operated at 6 mA. The overall emission appears white and is bright enough to be clearly observed by the naked eye in a normal light environment. The Commission International de I'Eclairage (CIE) color coordinates of the WLED are (0.32, 0.30), which are close to the optimal white light positioning, as displayed in Fig. 7d. Besides, other key device parameters including the color rendering index (CRI), color temperature (CCT), and power efficiency were measured to be 83.3, 7425 K, and 63.5 lm $W^{-1}$,

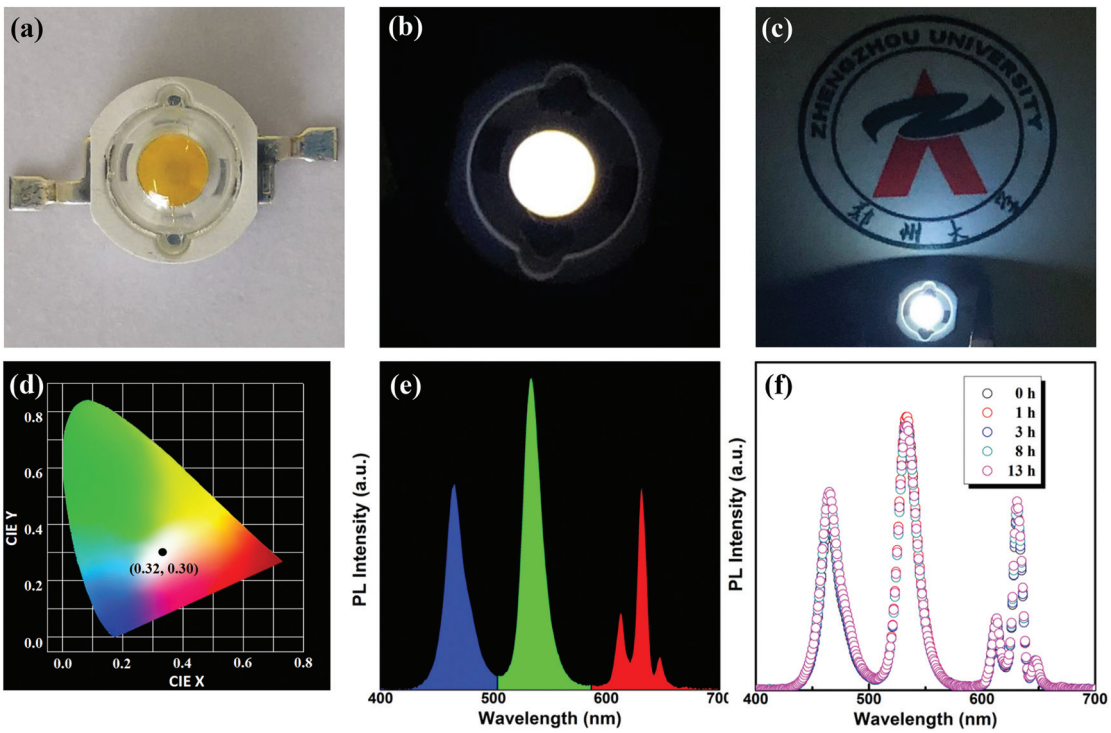


Fig. 7 (a) Image of the WLED device fabricated using $CsPbBr_3/SiO_2$ QD composites, KSF phosphors and a blue LED chip. (b) Photograph of the WLED operated at a driving current of 6 mA. (c) A logo of Zhengzhou University under WLED illumination. (d) CIE color coordinates of the WLED. (e) Emission spectrum of the WLED operated at 6 mA. (f) Emission spectra of WLEDs obtained after different running periods under the same bias and measurement conditions.

respectively. The efficiency value (63.5 lm $W^{-1}$) achieved here was much higher than those of the incandescent lamp (17 lm $W^{-1}$) and CdSe/$SiO_2$ QD monolith (47 lm $W^{-1}$).[34,43] Fig. 7e presents a typical emission spectra of the studied WLED at a driving current of 6 mA; three emission peaks at 460, 520 and 630 nm were resolved with no overlapping portions between them. The three emission components were in good correlation with the solid state PL peaks of the respective powders (Fig. S6, ESI†). On increasing the driving current from 6 to 36 mA, the green and red emission components increased accordingly, which implied that both phosphors demonstrate no saturation toward blue light excitation, as presented in Fig. S7 (ESI†).

It is generally accepted that long-term operation stability of perovskite-based optoelectronic devices has always been a challenge. To evaluate the device stability, the emission spectra of the WLED were obtained at different running periods in ambient air (25 °C, 35–50% humidity) with a fixed driving current of 6 mA. As shown in Fig. 7f, after 13 h continuous operation, the emission peak and spectra shape of the WLED remained unchanged, and the intensities of the three emission components were almost constant, thus demonstrating remarkable long-term stability. Fig. S8 (ESI†) displays a series of emission spectra of another reference WLED, in which the $CsPbBr_3/SiO_2$ QD powder was replaced by bare $CsPbBr_3$ QD powder. A sharp drop of the green emission component over running time could be observed, whereas the blue and red emission components remained unchanged. As a result, the CIE color coordinates of the reference WLED changed considerably after 13 h continuous operation (Fig. S9 and Table S1, ESI†). The above observations imply that the bare $CsPbBr_3$ QD powder is more sensitive to the blue excitation light than $CsPbBr_3/SiO_2$ QD composites, which is consistent with the above discussions on their photostability. Furthermore, the excellent device performance suggests that the $CsPbBr_3/SiO_2$ QD composites are better and reliable down-conversion phosphors for WLED applications.

## Conclusions

In conclusion, $CsPbBr_3$/silica QD composites were successfully prepared through a simple sol–gel reaction with TMOS as the molecule precursor. Compared with the results for fresh $CsPbBr_3$ QDs, substantially improved material stability against heat, light, and environmental oxygen/moisture was achieved. Moreover, the silica-coated $CsPbBr_3$ QDs possessed narrower PL linewidth and a higher PL quantum yield. These advantages allowed us to use the $CsPbBr_3$/silica QD composites as solid state phosphors for WLED applications. Finally, white light emission with CRI of 83.3, CCT of 7425 K, CIE coordinates of (0.32, 0.30), and high power efficiency of 63.5 lm $W^{-1}$ was obtained. More importantly, the proposed WLEDs demonstrated remarkable operation stability in ambient air in the continuous current mode. After a continuous operation for 13 h, no emission decay was observed, which was greatly superior to that of the reference device using bare $CsPbBr_3$ QD powder as the green phosphor. We believe that our study reported herein provides an effective strategy for improving the material stability of perovskite QDs, thereby endowing them with promising potentials in lighting and display applications.

## Conflicts of interest

There are no conflicts to declare.

## Acknowledgements

This work was supported by the National Natural Science Foundation of China (No. 11774318, 11604302, 61176044 and 11504331), the China Postdoctoral Science Foundation (2017T100535), the Key Scientific Research Projects of Higher Education in Henan Province (18A140007), the Support Program for Scientific and Technological Innovation Talents of Higher Education in Henan Province (19HASTIT017), the Outstanding Young Talent Research Fund of Zhengzhou University (1521317001), and the Startup Research Fund of Zhengzhou University (1512317003).

## Notes and references

1 M. Schreuder, K. Xiao, I. N. Ivanov, S. M. Weiss and S. J. Rosenthal, *Nano Lett.*, 2010, **10**, 573.
2 Z. Yuan, C. K. Zhou, J. Messier, Y. Tian, Y. Shu, J. Wang, Y. Xin and B. W. Ma, *Adv. Opt. Mater.*, 2016, **10**, 2009.
3 F. J. Zhang, J. Z. Song, B. N. Han, T. Fang, J. H. Li and H. B. Zeng, *Small Methods*, 2018, 1700382.
4 P. Waltereit, O. Brandt, A. Trampert, H. Grahn, J. Menniger, M. Ramsteiner, M. Reiche and K. Ploog, *Nature*, 2000, **406**, 865.
5 E. Jang, S. Jun, H. Jang, J. Lim, B. Kim and Y. Kim, *Adv. Mater.*, 2010, **22**, 3076.
6 S. Nakamura, *Science*, 1998, **281**, 956.
7 C. C. Lin and R. S. Liu, *J. Phys. Chem. Lett.*, 2011, **2**, 1268.
8 J. Chen, V. Hardev and J. Yurek, *Nanotechnol. Law Bus.*, 2014, **11**, 4.
9 Z. Shi, Y. Li, Y. Zhang, Y. Chen, X. Li, D. Wu, T. Xu, C. Shan and G. Du, *Nano Lett.*, 2017, **17**, 313.
10 Y. Tong, E. Bladt, M. F. Aygüler, A. Manzi, K. Z. Milowska, V. A. Hintermayr, P. Docampo, S. Bals and A. S. Urban, *Angew. Chem., Int. Ed.*, 2016, **55**, 13887.
11 G. Nedelcu, L. Protesescu, S. Yakunin, M. I. Bodnarchuk, M. J. Grotevent and M. V. Kovalenko, *Nano Lett.*, 2015, **15**, 5635.
12 L. Protesescu, S. Yakunin, M. I. Bodnarchuk, F. Krieg, R. Caputo, C. H. Hendon, R. X. Yang, A. Walsh and M. V. Kovalenko, *Nano Lett.*, 2015, **15**, 3692.
13 L. Song, X. Guo, Y. Hu, Y. Lv, J. Lin, Z. Liu, Y. Fan and X. Liu, *J. Phys. Chem. Lett.*, 2017, **8**, 4148.

 

14 A. Swarnkar, R. Chulliyil, V. K. Ravi, M. Irfanullah, A. Chowdhury and A. Nag, *Angew. Chem., Int. Ed.*, 2016, **54**, 15424.
15 J. Song, J. Li, X. Li, L. Xu, Y. Dong and H. Zeng, *Adv. Mater.*, 2016, **27**, 7162.
16 Z. F. Shi, Y. Li, S. Li, X. J. Li, D. Wu, T. T. Xu, Y. T. Tian, Y. S. Chen, Y. T. Zhang, B. L. Zhang, C. X. Shan and G. T. Du, *Adv. Funct. Mater.*, 2018, **28**, 1707031.
17 Y. Guo, K. Shoyama, W. Sato and E. Nakamura, *Adv. Energy Mater.*, 2016, **6**, 1502317.
18 S. Pathak, N. Sakai, F. W. R. Rivarola, S. D. Stranks, J. W. Liu, G. E. Eperon, C. Ducati, K. Wojciechowski, J. T. Griffiths, A. A. Haghighirad, A. Pellaroque, R. H. Friend and H. J. Snaith, *Chem. Mater.*, 2015, **27**, 8066.
19 G. Yang, Q. Fan, B. Chen, Q. Zhou and H. Zhong, *J. Mater. Chem. C*, 2016, **4**, 11387.
20 F. Palazon, Q. Akkerman, M. Prato and L. Manna, *ACS Nano*, 2017, **10**, 1224.
21 M. Meyns, M. Perálvarez, A. Heuer-Jungemann, W. Hertog, M. Ibáñez, R. Nafria, A. Genc, J. Arbiol, M. V. Kovalenko, J. Carrerras, A. Cabot and A. G. Kanaras, *ACS Appl. Mater. Interfaces*, 2016, **8**, 19579.
22 X. Li, Y. Wu, S. Zhang, B. Cai, Y. Gu, J. Song and H. Zeng, *Adv. Funct. Mater.*, 2016, **26**, 2584.
23 Y. Xu, Q. Chen, C. Zhang, R. Wang, H. Wu, X. Zhang, G. Xing, W. W. Yu, X. Wang, Y. Zhang and M. Xiao, *J. Am. Chem. Soc.*, 2016, **138**, 3761.
24 M. Müller, M. Kaiser, G. M. Stachowski, U. Resch-Genger, N. Gaponik and A. Eychmüller, *Chem. Mater.*, 2014, **26**, 3231.
25 D. S. Wuu, W. C. Lo, L. S. Chang and R. H. Horng, *Thin Solid Films*, 2004, **468**, 105.
26 S. W. Seo, E. Jung, C. Lim, H. Chae and S. M. Cho, *Appl. Phys. Express*, 2012, **5**, 035701.
27 Y. R. Do, D. H. Park and Y. S. Kim, *J. Electrochem. Soc.*, 2004, **151**, H210.
28 R. R. Pareja, R. L. Ibáñez, F. Martín, J. R. Ramos-Barrado and D. Leinen, *Surf. Coat. Technol.*, 2006, **200**, 6606.
29 H. C. Wang, S. Y. Lin, A. C. Tang, B. P. Singh, H. C. Tong, C. Y. Chen, Y. C. Lee, T. L. Tsai and R. S. Liu, *Angew. Chem., Int. Ed.*, 2016, **55**, 8056.
30 L. M. Xu, J. W. Chen, J. Z. Song, J. H. Li, J. Xue, Y. H. Dong, B. Cai, Q. S. Shan, B. N. Han and H. B. Zeng, *ACS Appl. Mater. Interfaces*, 2017, **9**, 26556.
31 A. Loiudice, S. Saris, E. Oveisi, D. T. L. Alexander and R. Buonsanti, *Angew. Chem., Int. Ed.*, 2017, **56**, 10696.
32 N. L. Rosi and C. A. Mirkin, *Chem. Rev.*, 2005, **105**, 1547.
33 S. Jun, J. Lee and E. Jang, *ACS Nano*, 2013, **7**, 1472.
34 S. Huang, Z. Li, L. Kong, N. Zhu, A. Shan and L. Li, *J. Am. Chem. Soc.*, 2016, **138**, 5749.
35 C. Sun, Y. Zhang, C. Ruan, C. Yin, X. Wang, Y. Wang and W. W. Yu, *Adv. Mater.*, 2016, **28**, 10088.
36 Q. X. Zhong, M. H. Cao, H. C. Hu, D. Yang, M. Chen, P. L. Li, L. Z. Wu and Q. Zhang, *ACS Nano*, 2018, **12**, 8579.
37 Z. Li, L. Kong, S. Huang and L. Li, *Angew. Chem., Int. Ed.*, 2017, **56**, 8246.
38 S. Jun, J. Lee and E. Jang, *ACS Nano*, 2013, **7**, 1472.
39 T. J. Savenije, C. S. Ponseca, L. Kunneman, M. Abdellah, K. Zheng, Y. Tian, Q. Zhu, S. E. Canton, I. G. Scheblykin, T. Pullerits, A. Yaresev and V. Sundström, *J. Phys. Chem. Lett.*, 2014, **5**, 2189.
40 S. Rudin, T. L. Reinecke and B. Segall, *Phys. Rev. B: Condens. Matter Mater. Phys.*, 1990, **42**, 11218.
41 Z. Shi, S. Li, Y. Li, H. Ji, X. Li, D. Wu, T. Xu, Y. Chen, Y. Tian, Y. Zhang, C. Shan and G. Du, *ACS Nano*, 2018, **12**, 1462.
42 Z. Li and X. Peng, *J. Am. Chem. Soc.*, 2011, **133**, 6578.
43 E. F. Schubert and J. K. Kim, *Science*, 2005, **308**, 1274.